# Photoionization of atomic magnesium including double-electron resonances

Zikri Altun*
*Jesse W. Beams Laboratory of Physics, University of Virginia, Charlottesville, Virginia 22901*
(Received 3 April 1989)

The photoionization cross sections of the $2s^2$, $2p^6$, and $3s^2$ subshells of atomic magnesium and angular distribution asymmetry parameters for the $2p^6$ subshell have been calculated using many-body perturbation theory. Double-electron resonance structure near the $3s$ threshold has been included. At higher energies, resonance structures due to the $2s \rightarrow np$ and $2p \rightarrow nd\,(ms)$ ($n \geq 3$, $m \geq 4$) excitations have also been included. The effects of spin-orbit interactions on the $2p \rightarrow nd\,(ms)$ resonances are examined. The calculated asymmetry parameter for the $2p^6$ subshell including the $2s \rightarrow np$ resonance structure is compared with the calculations of Deshmukh and Manson [Phys. Rev. A **28**, 209 (1983)].

## I. INTRODUCTION

There has been considerable interest among the theorists and experimentalists in the photoionization of atomic magnesium (Mg I). The cross section has been measured by Ditchburn and Marr,[1] Mehlman-Balloffet and Esteva,[2] Esteva, Mehlman-Baloffet, and Romand,[3] Baig and Connerade,[4] Preses, Burkhardt, Garver, and Leventhal,[5] and Fiedler, Kortenkamp, and Zimmerman.[6] These measurements were taken in the vicinity of the $3s$ threshold at 7.646 eV where the double-electron resonances due to the $3s^2(^1S) \rightarrow 3pnd\,(ms)(^1P)$ ($n \geq 3$, $m \geq 4$) excitations dominate. Calculations in this energy range were carried out by Bates and Altick[7] (configuration-interaction technique), Dubau and Wells[8] (close-coupling technique), Radojević and Johnson[9] (multiconfiguration Tamm-Dancoff technique), O'Mahony and Greene[10] ($R$-matrix technique), Rescigno[11] (complex–basis–function technique), and Moccia and Spizzo[12] ($L^2$ technique). A calculation by Dashmukh and Manson[13] using the relativistic random-phase approximation (RRPA) covered the region from the $3s$ threshold to 270 eV but included only the single-electron resonances due to the $2s \rightarrow np$ ($n \geq 6$) and $2p \rightarrow nd\,(ms)$ ($n \geq 8$, $m \geq 10$) excitations.

In this paper I present a detailed calculation of the photoionization cross section of atomic magnesium for photon energies ranging from the $3s$ threshold to 300 eV. The calculations were carried out using many-body perturbation theory (MBPT).[14–16] The double- and the single-electron resonances are incorporated through the coupled-equation method[17] which is essentially a close-coupling or $K$-matrix method.[18] The effect of the spin-orbit interaction on the $2p^5nd\,(ms)(^1P)\,J=1$ resonances is also examined. The angular asymmetry parameter $\beta$ for the $2p$ subshell was calculated including the effect of the $2s \rightarrow np$ resonances and is compared with various experiments and theory.

Section II includes a brief summary of the theory. Section III contains the results, and the conclusions are given in Sec. IV.

## II. THEORY

The photoionization cross section in the electric dipole approximation is given by[19]

$$\sigma(\omega)=\frac{4\pi}{c}\mathrm{Im}\alpha(\omega)\ , \tag{1}$$

where $\mathrm{Im}\alpha(\omega)$ is the imaginary part of the frequency-dependent dipole polarizability. Atomic units are used throughout this paper. Many-body perturbation theory is used to calculate the electric dipole matrix elements used in the evaluation of $\mathrm{Im}\alpha(\omega)$. The Hamiltonian is written

$$H=H_0+H_c\ , \tag{2}$$

where

$$H_0=\sum_{i=1}^{N}\left[-\frac{\nabla_i^2}{2}-\frac{Z}{r_i}+V(r_i)\right]\ , \tag{3}$$

and

$$H_c=\sum_{i<j=1}^{N}v_{ij}-\sum_{i=1}^{N}V(r_i)\ . \tag{4}$$

The term $v_{ij}$ represents Coulomb interactions between electrons $i$ and $j$. The single-particle potential $V(r_i)$ represents the average interaction of the $i$th electron with the remaining $N-1$ electrons, and $-Z/r_i$ is the interaction with the nucleus.

The dipole length matrix elements are given by

$$Z_L=\left\langle\psi_f\left|\sum_{i=1}^{N}z_i\right|\psi_0\right\rangle\ , \tag{5}$$

where $\psi_0$ and $\psi_f$ are many-particle ground and final states. The dipole velocity form is

$$Z_V=\frac{1}{E_0-E_f}\left\langle\psi_f\left|\sum_{i=1}^{N}\frac{d}{dz_i}\right|\psi_0\right\rangle\ , \tag{6}$$

 

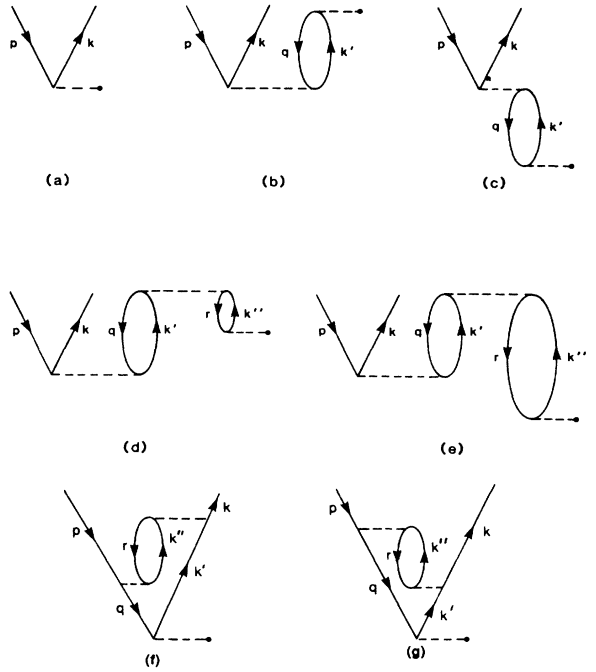


FIG. 1. Low-order Brueckner-Goldstone diagrams contributing to the dipole matrix element for photoionization. Time proceeds from bottom to top in these diagrams. Lines with arrows pointing down represent hole states and lines with arrows pointing up represent particle states. (a) Lowest-order dipole. (b) Ground-state correlation (GSC) diagram. (c) Final-state correlation (FSC) diagram. (d)–(k) Second-order diagrams. Dashed line ending with an isolated solid dot indicates matrix element of $z$. Other dashed lines represent the electron-correlation interaction. Exchange diagrams are assumed to be included but are not explicitly shown.

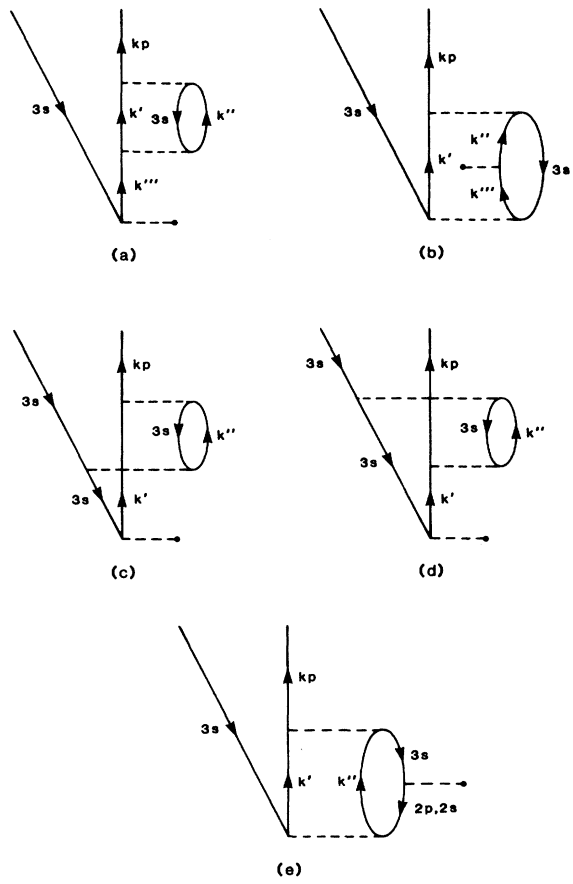


FIG. 2. Second-order diagrams representing the correlations due to the excitations of two $3s$ electrons.

where $E_0$ and $E_f$ are energy eigenvalues corresponding to $\psi_0$ and $\psi_f$, respectively. The velocity and length forms are equal if the wave functions are exact eigenfunctions of $H$ of Eq. (2).

The lowest-order MBPT diagrams contributing to $Z_L$ or $Z_V$ are shown in Fig. 1. In this case the transition involves the excitation of an electron from orbital $p$ occupied in $\psi_0$ to orbital $k$ occupied in $\psi_f$. In these diagrams, lines with arrows drawn upward represent occupied excited single-particle states and are called particles, and those with arrows pointing downward represent unoccupied unexcited states and are called holes. The correlation interaction $H_c$ is represented by dashed lines between particle and hole lines. The dipole interaction is represented by a dashed line ending with a solid dot. The order of a diagram corresponds to the number of interactions with $H_c$, and the diagrams are read from bottom to top. Diagrams in which the $H_c$ interactions precede the dipole interaction are said to contribute to the ground-state correlations (GSC). When the dipole interaction occurs first, the diagram is said to contribute to the final-state correlations (FSC).

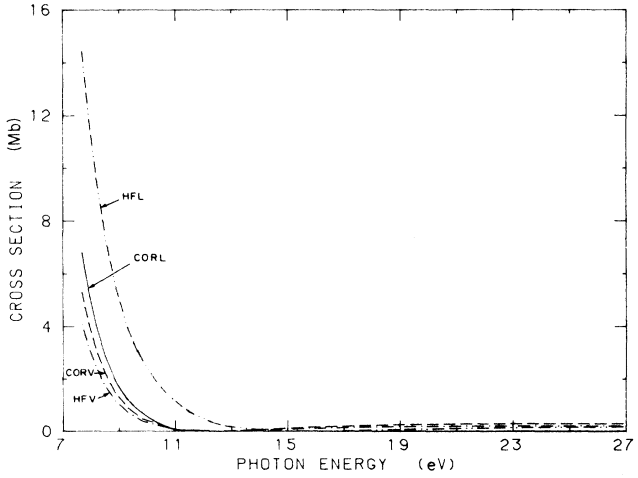


FIG. 3. Photoionization cross section calculated for the $3s^2 \rightarrow 3skp\,(^1P)$ transition not including resonance contributions. The curves labeled HFL and HFV represent the length and velocity cross sections in the Hartree-Fock approximation. Curves CORL and CORV are correlated length and velocity results without the contribution from the double excitations of two $3s$ electrons.

The Hamiltonian with spin-orbit interaction may be written as

$$H_{\mathrm{SO}}=H+\sum_{i=1}^{N}\zeta_{n_i l_i}(LSJ)\mathbf{l}_i\cdot\mathbf{s}_i\ , \tag{7}$$

where $\zeta_{n_i l_i}(LSJ)$ are the effective spin-orbit parameters defined by Blume and Watson.[20] Specifically, we examine the effect of the spin-orbit interaction on the $2p^5md$ and $2p^5ms$ states with $J=1$. The spin-orbit interaction mixes the $^1P_1$ multiplet with other $^{2S+1}L_J$ multiplets with $J=1$. The mixing coefficients are obtained by diagonalizing $H_{\mathrm{SO}}$ using $|LSJM_J\rangle$ basis states.[20–22] The resulting states are then treated as bound excited states for the $2p$ subshell.

The diagram of Fig. 1(c) with $p=3s$, $k=kp$, $q=2s(2p)$, and $k'=np(nd,ns)$ contributes to single-electron resonances in the $3s$ cross section in lowest order. The lowest-order double-electron resonances in the $3s$ cross section are represented by the diagrams of Fig. 2. These diagrams are second order in the Coulomb interaction as compared with the diagram of Fig. 1(c) which is in first order in the Coulomb interaction. These diagrams have a series of simple poles at the positions of the resonances which may be handled by summing higher-order diagrams to infinite order.[21,23] In this work we used the coupled-equation method[17] to account for correlations in the final state. In forming the coupled equations, we used nine excited configurations given by $2skp$, $2p^5kd(ks)$, $3skp$, $3pkd(ks)$, $3dkf(kp)$, and $4skp$, all with $^1P$ final coupling. Here $ks$, $kp$, $kd$, and $kf$ refer to both bound and continuum states. Solving the coupled equations is equivalent to including the interactions among these final-state channels to infinite order and is equivalent to a $K$-matrix calculation.[18] Application of the coupled-equation method[17] to calculate the resonance structure effectively results in real and imaginary shifts to the denominators of the lowest-order FSC diagrams which prevent singularities. The imaginary shift is related to the full width at half maximum of the resonance state and the real shift affects the position of the resonance.[17] The expression used in the calculation of the photoelectron angular distribution asymmetry parameter $\beta(\omega)$ has been published elsewhere.[18,24–26]

## III. CALCULATIONS AND RESULTS

The ground-state orbitals of Mg I were obtained from a self-consistent Hartree-Fock (HF) calculation[27] and were not changed during the rest of the calculation. All singly excited bound and continuum orbitals originating from the $2s$, $2p$, and $3s$ subshells were then calculated in the same frozen-core HF $V^{N-1}$ potential for a given $l$. The doubly excited continuum and bound $ks$, $kd$, $kf$, and $kp$ orbitals were calculated in frozen-core Hartree-Fock $V^{N-1}$ potentials derived from the couplings $2p^63pks(kd)(^1P)$, $2p^63dkf(kp)(^1P)$, and $2p^64skp(^1P)$. The radial $3p$, $3d$, and $4s$ orbitals were calculated in frozen-core $2p^6$ Hartree-Fock $V^{N-2}$ potentials.[16] For each angular momentum, 10 bound and 42 continuum orbitals were calculated with appropriate projection operators when necessary to ensure the orthogonality of the excited-state orbitals to ground-state orbitals of the same angular momentum.[28,29] The effect of the remainder of

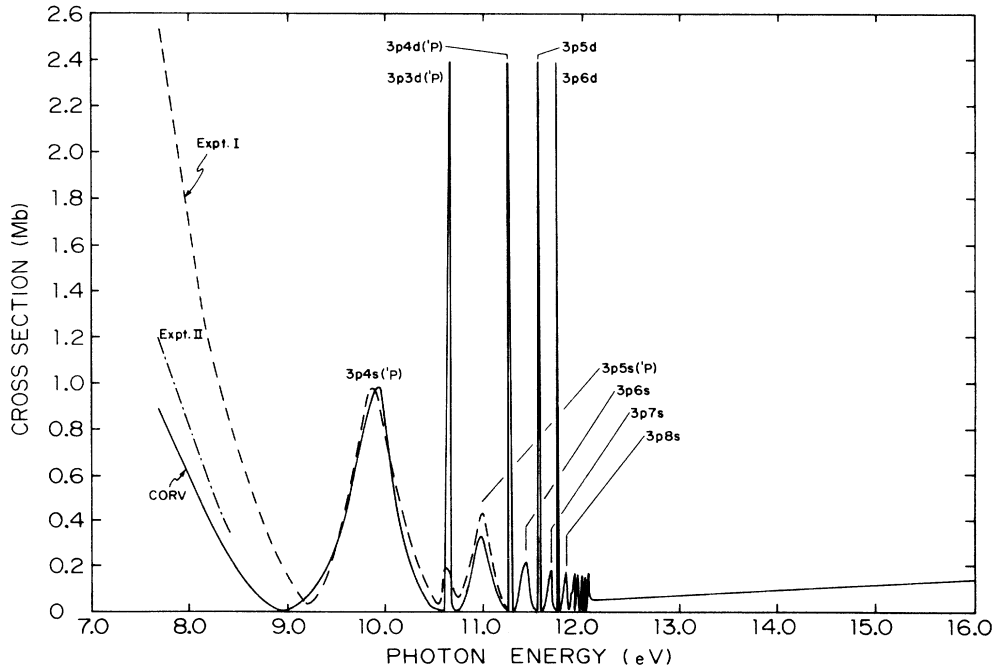


FIG. 4. Photoionization cross section for the $3s^2\rightarrow 3skp(^1P)$ transition involving the double-electron resonances as a function of photon energy. ——, MBPT velocity calculation (CORV), this work; — — —, measurement (Expt. I) by Preses *et al.*, Ref. 5.; —·—·—·, measurement by Ditchburn and Marr (Expt. II), Ref. 1. Double-electron resonances are labeled.

the bound excited states was taken into account by the $n^{-3}$ rule[16] for diagrams contributing to correlations on the ground states. For diagrams contributing to correlations in the final states, higher bound states were included by explicit calculation and a back extrapolation of the continuum below the first $K$-mesh value into the bound region.[17]

Calculations of the photoionization cross section for the $3s$ valence shell from the threshold to 27 eV, not including effects of double excitations, are given in Fig. 3. The curves labeled HFL and HFV represent the length and velocity forms of the cross section in the HF approximation. These cross sections have a large disagreement not only in their magnitudes but also in the positions of Cooper minima.[30] We have studied the effects of the correlations on these cross sections in two steps. In the first step we did not include the diagrams of Fig. 2 for the two $3s$ electrons. Diagrams included are shown in Figs. 1(b)–1(g). The labelings of the hole and particle lines in these diagrams were taken to be among the $2s$, $2p$, and $3s$ excitations. Threshold energies used in correlating the ground state are the HF frozen-core values, which for the $3s$, $2p$, and $2s$ hole states are, respectively, 0.2534, 2.2882, and 3.7801 a.u. In correlating the final state, experimental removal energies, which are 0.281 09, 2.1258, and 3.5477 a.u.,[31] were used, respectively, for these hole states. Excited bound orbital energies were taken to be HF frozen-core calculated values. Final-state correlations were calculated by solving the coupling equations only for the $2skp(^1P)$, $2p^5kd(ks)(^1P)$, and $3skp(^1P)$ channels. In these equations modified Coulomb grids were used to account for diagrams 1(d), 1(e), 1(f), and 1(g). The modified Coulomb grids were obtained by first summing over the $k''$ states in these diagrams and then adding them to the Coulomb grid of the diagram in Fig. 1(c). The dipole matrix elements used as input to the coupled equations were taken to be the sum of the HF results plus corrections due to the correlations in the ground state as shown in Fig. 1(b). The length and velocity results obtained from this first step are shown in Fig. 3 in the curves labeled CORL (correlated length) and CORV (correlated velocity), respectively. There is now considerable agreement between CORL and CORV calculations which agree with the RRPA results of Deshmukh and Manson.[13] They both have the Cooper minimum at the same position (11.63 eV) and the correlations brought the threshold cross sections from 14.41 Mb (HFL) and 4.06 Mb (HFV) to 6.10 Mb (CORL) and 5.20 Mb (CORV). However, the results near the threshold are still far from the measurements.[1–6]

In the next step we considered the correlations due to the simultaneous excitation of the two $3s$ electrons. We extended the coupled equations used in the first step to include those diagrams in Fig. 2 with the doubly excited intermediate states $3pkd(ks)$, $3dkf(kp)$, and $4skp$ all coupled to $^1P$. When $kp$, $kd$, and $kf$ refer to bound excited orbitals, the corresponding denominators may vanish when the excitation energy of the $3s \rightarrow kp$ transition is degenerate with the excitation energy of the doubly excited states. When this happens diagrams are said to contribute to the double-electron resonances. In this calculation, the doubly excited bound configuration used as intermediate states are $3pnd(ms)(^1P)$, $3dnp(mf)(^1P)$, and $4snp(^1P)$ ($n=3-12$, $m=4-13$). All of these states lies above the ionization threshold and appear as autoionization resonances in the $3s$ cross section. In extending the coupled equations, we used experimental thresholds for all the continuum channels and HF single-particle ener-

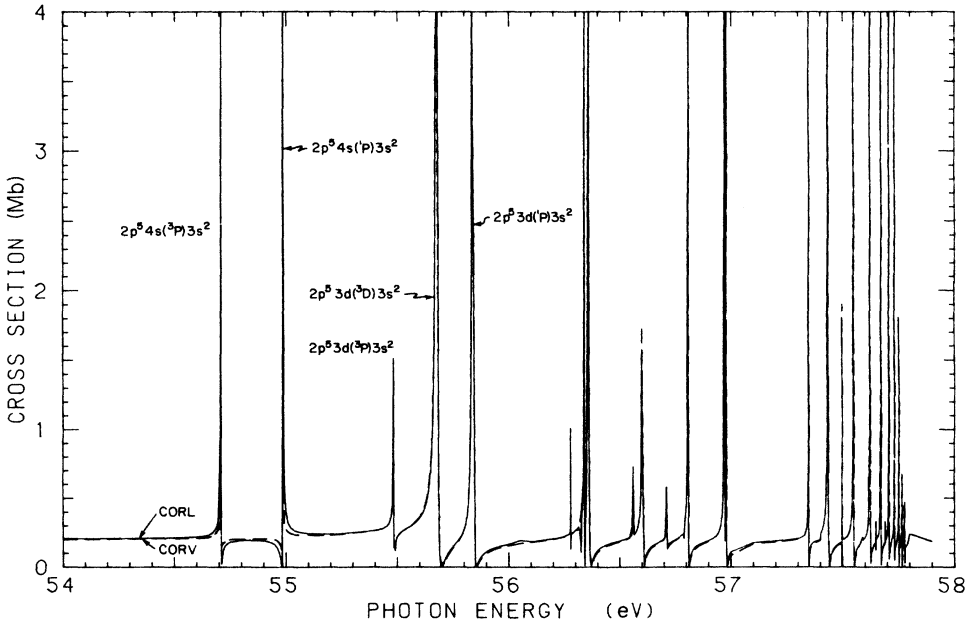


FIG. 5. Correlated length (solid line) and velocity (dashed line) cross sections for the $3s^2 \rightarrow 3skp(^1P)$ transition in the $2p \rightarrow nd, ns$ resonance region including spin-orbit effects.

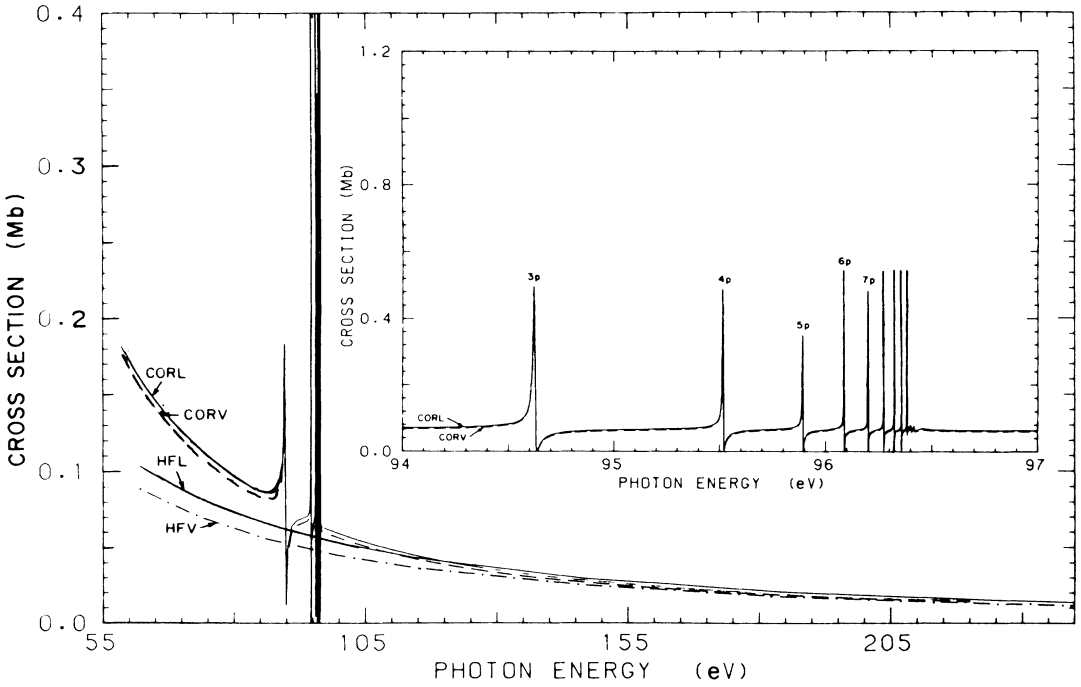


FIG. 6. Hartree-Fock and correlated partial $3s$ photoionization cross sections beyond the $2p$ threshold. The HFL and HFV curves represent the Hartree-Fock length and velocity cross sections. The curves CORL and CORV are correlated length and velocity MBPT calculations. The resonances which are shown in an expanded scale inside the box are due to $2s \rightarrow np$ excitations.

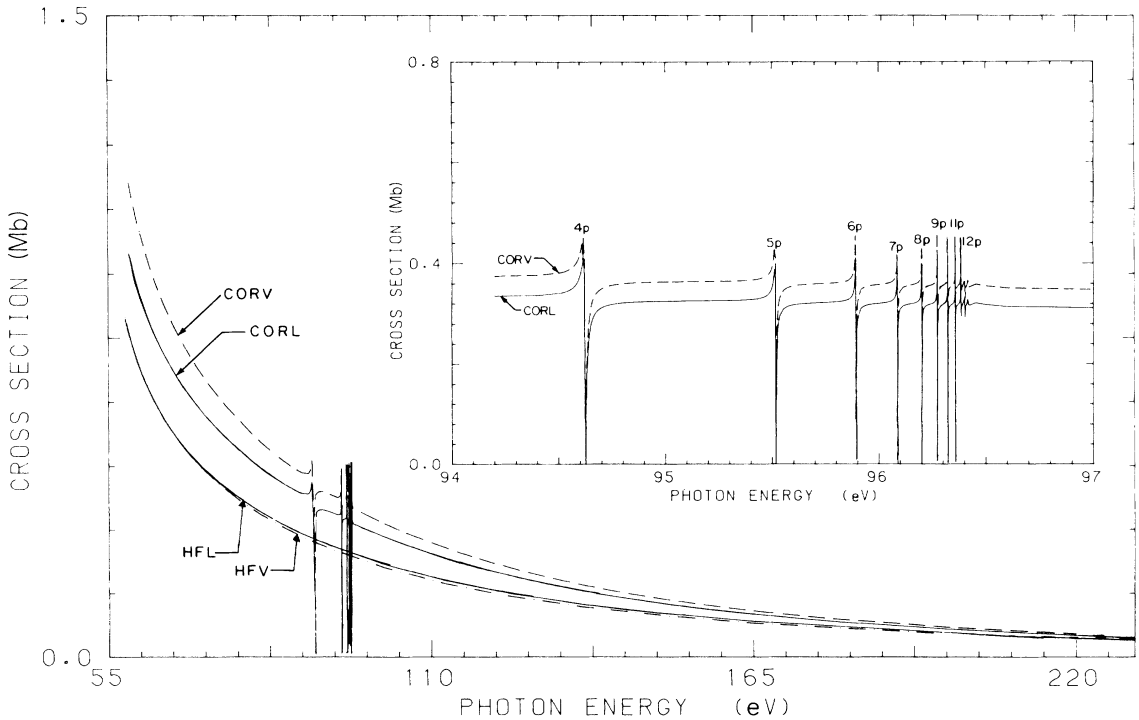


FIG. 7. Hartree-Fock and correlated partial $2p \rightarrow ks$ photoionization cross sections. The HFL and HFV curves represent the Hartree-Fock length and velocity cross sections. The curves CORL and CORV are correlated length and velocity MBPT calculations. The resonances, which are shown in an expanded scale inside the box, are due to $2s \rightarrow np$ excitations.

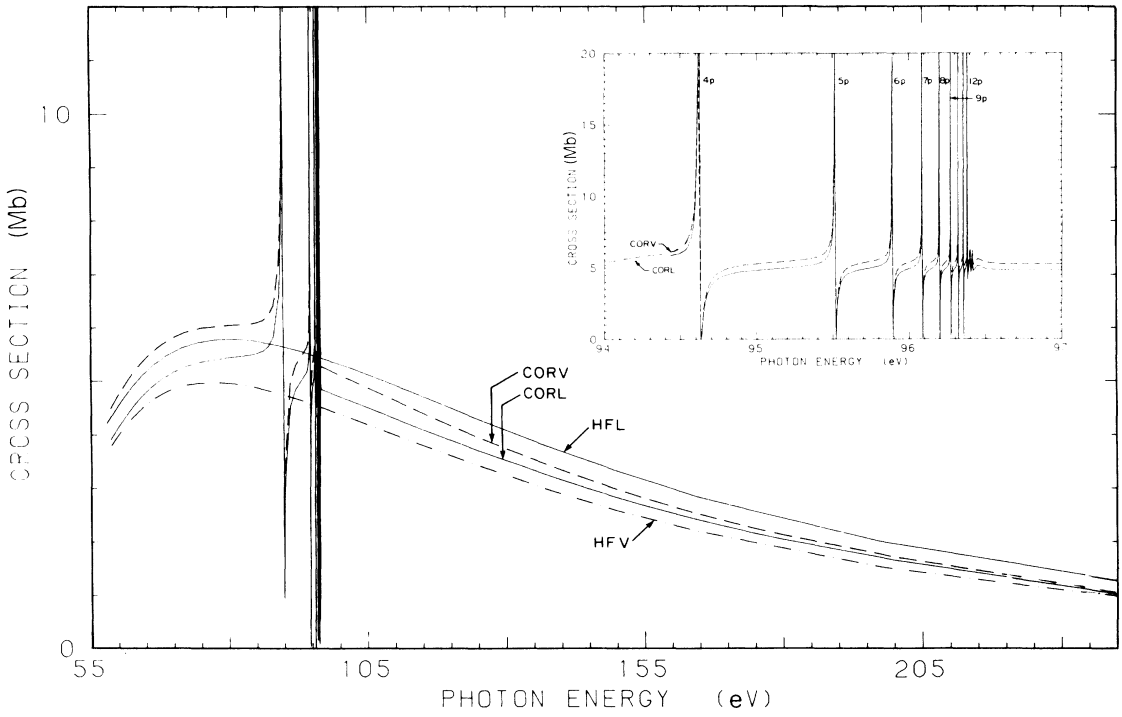


FIG. 8. Hartree-Fock and correlated partial $2p \rightarrow kd$ photoionization cross section. The HFL and HFV curves represent the Hartree-Fock length and velocity cross sections. The curves CORL and CORV are correlated length and velocity MBPT calculations. The resonances which are shown in an expanded scale inside the box are due to the $2s \rightarrow np$ excitations.

gies for the bound excited states. The experimental thresholds for the $3s^2 \rightarrow 3pkd\,(kf)(^1P)$, $3dkf\,(kp\,(^1P)$, and $4skp\,(^1P)$ transitions are 0.4438, 0.606 56, and 0.598 97 a.u., respectively.[32] The diagram of Fig. 2(c) represents relaxation and we found it to be very important for this calculation. The relaxation effects can also be accounted for by calculating excited orbitals in the field of the relaxed ionic core.[33–35] The sum and integral over $k'''$ states in the diagram of Fig. 2(b) was obtained by a differential equation technique[36] before it was used as an input to the coupled equations.

We compare our final correlated velocity cross section (CORV) with measurements by Preses *et al.*[5] [experiment I (Expt. I)] and Ditchburn and Marr[1] (Expt. II) for the $3s \rightarrow kp$ channel in Fig. 4. The resonances in the curves

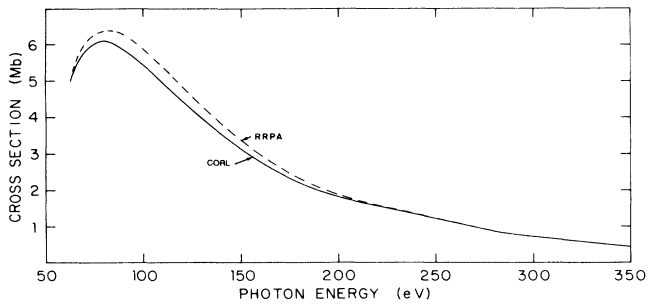


FIG. 9. Total photoionization cross section of the $2p^6$ subshell of magnesium as a function of photon energy. The curve labeled CORL is correlated length result. The curve labeled RRPA is relativistic random-phase approximation result from Ref. 13.

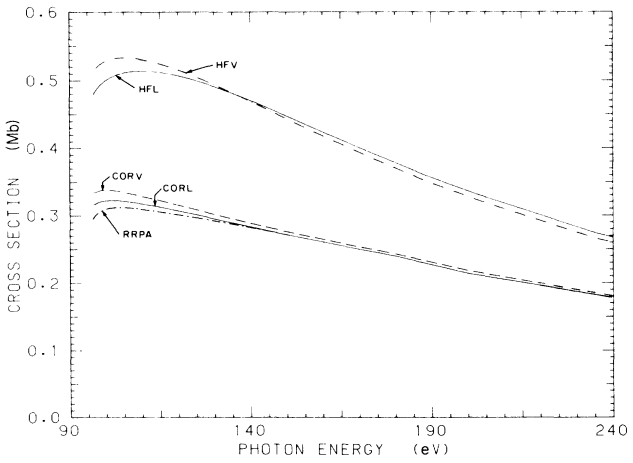


FIG. 10. Hartree-Fock and correlated partial 2*s* photoionization cross section. The HFL and HFV curves represent the Hartree-Fock length and velocity cross sections. The curves CORL and CORV are correlated length and velocity MBPT calculations. The RRPA results are from Ref. 13.

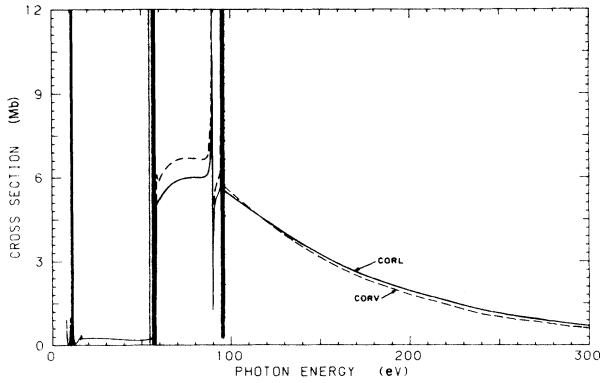


FIG. 11. Total $2s+2p+3s$ photoionization cross section from the first ionization threshold to 240 eV in both the length (solid line) and velocity (dashed line) forms.

(CORV, Expt. I) are due to the $3s^2(^1S)\rightarrow 3pns(^1P)$ and $3pnd(^1P)$ transitions. In comparing our results with those of Preses *et al.*[5] we normalized their data to ours at the peak of the first resonance ($3p4s\ ^1P$). Using this normalization, our calculation is not in good agreement with the measurement of Preses *et al.*[5] from the threshold to the minimum in the low-energy side of the $3p4s(^1P)$ resonance. However, the only absolute measurement[1] done thus far in this region is in good agreement with our result. As may be seen from Fig. 4, our threshold value for the $3s$ cross section is 0.92 Mb (CORV) as compared to the experimental values 2.55 Mb (Expt. I) and 1.20 Mb (Expt. II). Threshold values given by Bates and Altick,[7] Dubau and Wells,[8] Moccia and Spizzo,[12] O'Mahony and Greene,[10] and Rescigno[11] are 2.55, 1.5, 2.20, 4.3, and 2.3 Mb, respectively. The relaxation diagram of Fig. 2(c) was found to be the major cause of the significant reduction near the threshold. We have not presented our correlated length result in Fig. 4 since it is in good agreement with the velocity result everywhere except in the near-threshold region. The threshold value of the length cross section is 0.57 Mb, which is about half of the experimental result of Ditchburn and Marr.[1]

Figure 5 contains our correlated length and velocity calculations of the $3s\rightarrow kp$ cross section in the $2p\rightarrow nd$, $ns$ resonance region. We calculated ten bound resonance states for both $nd$ and $ns$ excitations and included the effects of spin-orbit interactions on the first four of these states. The spin-orbit interaction mixes the $^1P_1$, $^3P_1$, and $^3D_1$ terms of each $nd$ resonance and $^1P_1$ and $^3P_1$ terms of each $ns$ resonance. The mixed states in which the multiplet $2p^5ns(^1P_1)$ is strongest were always found to be the highest in energy. The transition from the ground state to the mixed states of $ns$ resonances exhibits a 3:2 intensity ratio ($^1P_1$:$^3P_1$) for $ns=4s$ and 2:1 for $ns=5s-7s$. The mixed states in which the multiplets $2p^5nd(^1P_1)$ and $2p^5nd(^3P_1)$ dominate were found to be the highest and lowest, respectively, in energy for $nd=3d-5d$, with $2p^5nd(^3D_1)$ always in the middle. For $nd=6d$, the $^1P_1$ is the lowest and $^3P_1$ is the highest in energy. The transitions from the ground state to the mixed states of $nd$ resonances exhibit a 7:4:1 intensity ratio ($^1P$:$^3D$:$^3P$) for $nd=3d$; 3:2:1 for $nd=4d,5d$, 2:2:1 for $nd=6d$. The recent calculation of Deshmukh and Manson[13] also included these resonances except for the first three of the $nd$ and four of the $ns$ resonances. Thus far we are not aware of any experiment in this region.

In Fig. 6 we present the partial $3s\rightarrow kp$ cross sections above the $2p$ threshold (58.7 eV). The resonances in the

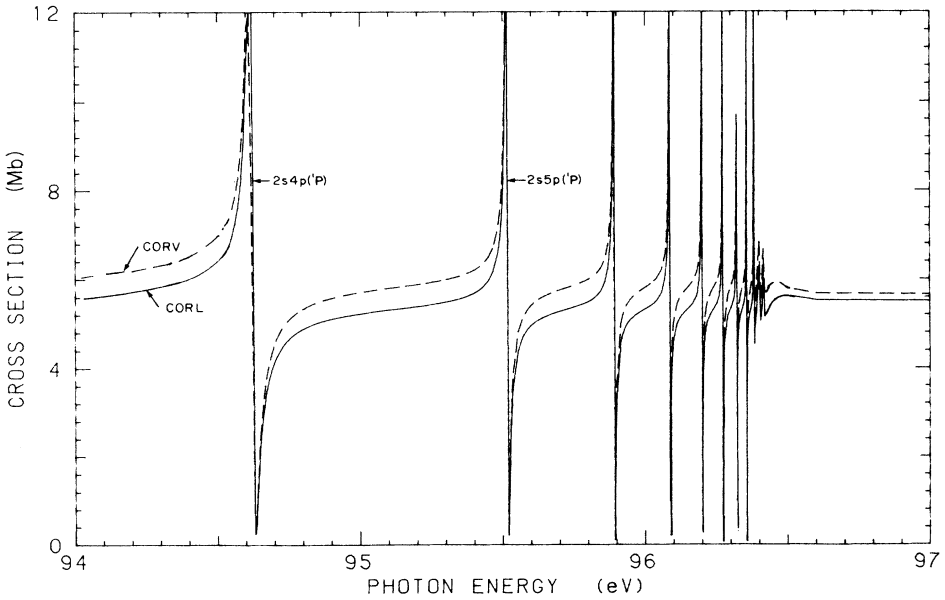


FIG. 12. Total $2s+2p+3s$ cross section in the region of the $2s\rightarrow np$ ($n\geq 3$) resonances. The solid line is the MBPT length calculation. The dashed line is the MBPT velocity calculation.

correlated length and velocity cross sections are due to $2s \rightarrow np$ excitations. The resonances in the figure within the box represent some of these resonances in an extended scale. These resonances show typical asymmetric Fano[30] line shapes. The widths of these resonances also include contributions from decay to other continuum channels corresponding to the ionization of the $2p$ electrons. The curves labeled HFL and HFV in Fig. 6 represent the length and velocity results in the HF approximation.

The partial cross sections obtained for the $2s$ and $2p$ subshells from the solution of the coupled equations are shown in Figs. 7–10. The coupled-equation length and velocity partial cross sections for both the $2s$ and the $2p$ shells are found to be in excellent agreement in all cases. The partial photoionization cross section for the $2p \rightarrow ks$ channel is shown in Fig. 7. The curves labeled HFL and HFV in these figures represent the lowest-order length and velocity calculations. The correlated length and velocity cross sections in the same figures are labeled CORL and CORV, respectively. The resonances in the CORL and CORV curves are due to $2s \rightarrow np$ excitations. The figure within the box represents some of these resonances in an extended scale. However, these resonances are much stronger in the $2p \rightarrow kd$ cross section, as will be discussed below. The correlations increased both the CORL and CORV cross sections compared to the HFL and HFV results.

In Fig. 8 we present the correlated length and velocity $2p \rightarrow kd$ partial cross sections (CORL,CORV) along with the lowest-order results (HFL,HFV). The resonances again are due to $2s \rightarrow np$ excitations. The figure within the box represents some of these resonances in an extended scale. These resonances are much stronger in the $2p \rightarrow kd$ channel than in either of the $3s \rightarrow kp$ and $2p \rightarrow ks$ channels. The correlations brought the length and velocity results close to each other by pushing both of them up below the resonances and pushing the velocity up and length down above the resonances compared to the HFL and HFV results.

We compare our correlated total length cross sections (CORL) for the $2p$ subshell with the recent calculation of Deshmuhk and Manson[13] (RRPA) in Fig. 9. In comparing our result with the RRPA curve, we averaged over the $2s \rightarrow np$ resonances. The agreement between two calculations is good. This is not surprising because both calculations included the most important correlations due to the single excitations from the $2s$, $2p$, and $3s$ shells with the same degree of approximation in this region.

In Fig. 10 we compare our correlated $2s \rightarrow kp$ length and velocity cross sections (CORL,CORV) with the RRPA calculation of Deshmukh and Manson and with Hartree-Fock calculations. The agreement between the many-body calculations and the RRPA calculations is excellent. The reduction in the CORL and CORV cross sections compared to the HFL and HFV curves was found to be mainly due to the interchannel interaction with the $2p \rightarrow kd$ channel.

We present the sum of the correlated $2s$, $2p$, and $3s$ partial cross sections in both length (CORL) and velocity (CORV) approximations in Fig. 11. The resonance region between 90–97 eV is extended and replotted in Fig. 12.

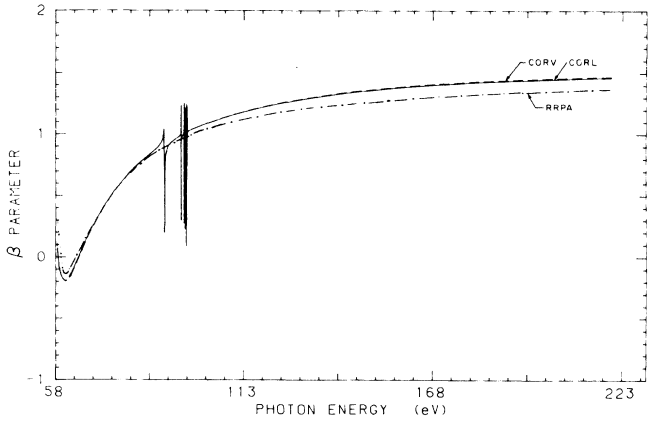


FIG. 13. The angular asymmetry distribution parameter as a function of photon energy for photoelectrons from the $2p^6$ subshell. Correlated length (CORL) and velocity (CORV) calculations using MBPT including $2s \rightarrow np$ resonances. Dot-dashed line indicates calculation by RRPA method, Ref. 13.

The angular distribution asymmetry parameter $\beta(\omega)$ for the photoionization from the $2p$ subshell of atomic magnesium has been calculated in both length and velocity approximations. The two forms are in excellent agreement. Our length (CORL) and velocity (CORV) curves are compared with the RRPA calculation of Deshmukh and Manson[13] in Fig. 13, and are in good agreement. In our calculation of $\beta(\omega)$ we used correlated dipole matrix elements obtained from our nine-channel coupled equations which also includes the effects of the $2s \rightarrow np$ resonances. The rapid variation in the asymmetry parameter as a function of photon energy in the near-threshold region is mainly due to the strong interference between the $2p \rightarrow kd$ and $2p \rightarrow ks$ channels.

## IV. DISCUSSION AND CONCLUSIONS

Many-body perturbation theory has been used to treat electron correlations including relaxation effects and single- and double-electron resonances in the photoionization of the magnesium atom over a wide energy range. This work used nine coupled final-state channels originating from $2s$, $2p$, and $3s$ single excitations and the double excitations of the two $3s$ electrons. I have included first- and higher-order correlations in the ground state and spin-orbit splitting of the lower members of the $2p \rightarrow nd\,(ns)$ resonances. The $3s$ threshold region is dominated by double-electron resonances, particularly $3pns\,(^1P)$ $(n \geq 4)$ and $3pnd\,(^1P)$ $(n \geq 3)$. The value of the $3s$ cross section at the threshold is 0.92 Mb (length) and 0.57 Mb (velocity) compared to the previous calculations[7–13] which give values between 1.5–4.3 Mb as discussed. I also included correlations from the $2s$ and $2p$ subshells which are found to be quite significant in this calculation. Our threshold results for the $3s$ cross section appear low by about a factor of 2, as compared with the

other calculations,[7-11] which agree very well in shape with the recent (unnormalized) experiment by Preses *et al.*[5] Our results at threshold are very sensitive to the choice of threshold energy and in the curve presented in Fig. 4 the experimental threshold energy was used. When the Hartree-Fock single-particle energy for the $3s$ ionization energy is used, the cross section at the threshold is approximately 3.0 Mb, in better agreement with the other calculations and the experiment by Preses *et al.*[5] The agreement between the length result and the absolute measurement by Ditchburn and Marr[1] near the threshold is reasonable. However, the threshold value obtained from the experiment of Preses *et al.*[5] is about a factor of 2.5 times larger than ours. This value is obtained by normalizing the experiment of Preses *et al.*,[5] either to the peak of the $3p4s(^1P)$ resonance as calculated by Bates and Altick[7] or by us. The relative heights of the $3p5s(^1P)$ and $3p6s(^1P)$ resonances given by the measurement of Fiedler, Kortenkamp, and Zimmermann,[6] which did not include the region below the low-energy side of the $3p3d(^1P)$ resonance, are consistent with our calculations and the previous calculations.[7-11]

The total cross section does not include contributions from the photoionization with excitation and double photoionization of the two $3s$ electrons. We plan to calculate these cross sections in future work.

The results of this work above the double-electron resonance region in the $3s$ cross section are in quite good agreement with the RRPA calculations.[13] This calculation indicates that many-body theory is useful in calculating photoionization cross sections and angular distribution asymmetry parameters including correlations over a wide energy range and is not limited to the threshold region.

## ACKNOWLEDGMENTS

I wish to thank Dr. H. P. Kelly, Dr. Daniel Frye, and Mickey Kutzner for helpful discussions. We are very grateful to the National Science Foundation for support under Grant No. INT-8507760 and Grant No. PHY-8705545-01.

---

*Permanent address: Marmara Universitesi, Fen-Ed. Fakültesi Istanbul, Turkey.

[1]R. W. Ditchburn and G. B. Marr, Proc. Phys. Soc. London, Sect. A **66**, 655 (1953).
[2]G. Mehlman-Balloffet and J. M. Esteva, Astrophys. J. **157**, 945 (1969).
[3]J. M. Esteva, G. Mehlman-Balloffet, and J. Romand, J. Quant. Spectrosc. Radiat. Transfer **12**, 1291 (1972).
[4]A. Baig and J. P. Connerade, Proc. R. Soc. London, Ser. A **364**, 353 (1978).
[5]M. Preses, C. E. Burkhardt, W. P. Garver, and J. J. Leventhal, Phys. Rev. A **29**, 985 (1984).
[6]W. Fiedler, Ch. Kortenkamp, and P. Zimmermann, Phys. Rev. A **36**, 384 (1987).
[7]G. N. Bates and P. L. Altick, J. Phys. B **6**, 653 (1973).
[8]J. Dubau and J. Wells, J. Phys. B **6**, L31 (1973).
[9]V. Radojević and W. R. Johnson, Phys. Rev. A **31**, 2991 (1985).
[10]P. F. O'Mahony and C. H. Greene, Phys. Rev. A **31**, 250 (1985).
[11]T. N. Rescigno, Phys. Rev. A **31**, 607 (1984).
[12]R. Moccia and P. Spizzo, J. Phys. B **21**, 1133 (1973).
[13]P. C. Deshmukh and S. T. Manson, Phys. Rev. A **28**, 209 (1983).
[14]K. A. Brueckner, Phys. Rev. **97**, 1353 (1955).
[15]J. Goldstone, Proc. R. Soc. London, Ser. A **239**, 267 (1957).
[16]H. P. Kelly, Adv. Theor. Phys. **2**, 75 (1968).
[17]E. R. Brown, S. L. Carter, and H. P. Kelly, Phys. Rev. A **16**, 1525 (1977).
[18]A. F. Starace, in *Corpuscles and Radiation in Matter I,* Vol. 31 of *Handbuch der Physik,* edited by W. Melhorn (Springer-Verlag, Berlin, 1982), p. 1.
[19]U. Fano and J. W. Cooper, Rev. Mod. Phys. **40**, 441 (1968).
[20]M. Blume and R. E. Watson, Proc., R. Soc. London, Ser. A **270**, 127 (1962).
[21]Z. Altun, S. L. Carter, and H. P. Kelly, Phys. Rev. A **27**, 1943 (1983).
[22]D. Frye and H. P. Kelly, Phys. Rev. A **11**, 5143 (1987).
[23]S. L. Carter and H. P. Kelly, Phys. Rev. A **13**, 1388 (1976).
[24]J. W. Cooper and R. N. Zare, in *Lectures in Theoretical Physics,* Vol. XI-C of *Atomic Collision Processes,* edited by S. Geltman, K. Mahanthoppa, and W. Brittin (Gordon and Breach, New York, 1969).
[25]M. Ya. Amusia and N. A. Cherepkov, Case Stud. At. Phys. **5**, (2) 47 (1975).
[26]A. Burgess, Proc. Phys. Soc. London **81**, 442 (1963).
[27]C. Froese-Fischer, Comput. Phys. Commun. **14**, 145 (1978).
[28]S. Huzinaga and C. Arnau, Phys. Rev. A **1**, 1285 (1970).
[29]J. H. Silverstone and M. L. Yin, J. Chem. Phys. **49**, 2026 (1968).
[30]U. Fano and J. W. Cooper, Rev. Mod. Phys. **40**, 441 (1968).
[31]W. Melhorn, in *Corpuscles and Radiation in Matter I,* Vol. 31 of *Handbuch der Physik,* edited by W. Melhorn (Springer-Verlag, Berlin, 1982).
[32]C. E. Moore, *Atomic Energy Levels,* Natl. Bur. Stand (U.S.) Circ. No. 467 (U.S. GPO, Washington, D.C., 1971) Vol. 1.
[33]M. Ya. Amusia, V. K. Ivanov, and L. V. Chernysheva, Phys. Lett. **59A**, 191 (1976).
[34]H. P. Kelly and Z. Altun, in *Giant Resonances in Atoms, Molecules, and Solids,* Vol. 151 of *NATO Advanced Study Institute, Series B: Physics,* edited by J. P. Connerade (Plenum, New York, 1986).
[35]S. L. Carter and H. P. Kelly, Phys. Rev. A **24**, 170 (1981).
[36]A. Dalgarno and J. T. Lewis, Proc. R. Soc. London, Ser. A **233**, 70 (1955); R. M. Sternheimer, Phys. Rev. **96**, 951 (1954).